PAPER

Check for updates

Stability of neutral molecular polynitrogens: energy content and decomposition mechanisms†

A. C. R. Gomes, [ID] [a] M. X. Silva [ID] [b] and B. R. L. Galvão [ID] *[a]

The potential application of all-nitrogen molecules as high energy density materials (HEDMs) has been attracting considerable scientific effort. If stable enough to be synthesized and stored, these systems may be used as a green source of energy. However, it is very difficult to obtain these structures under mild experimental conditions. Theoretical chemistry may aid in the search for polynitrogens that are more likely to have experimental usability. The barriers towards decomposition are an effective way to assess their stability, but these have not been thoroughly studied. Most of the previous effort in this direction focus on a single N_x case, each employing different accuracy levels, and the decomposition of caged structures has been little explored. Here we explore the stability and decomposition of several neutral molecular polynitrogens of different sizes and shapes using a common and accurate theoretical framework in order to compare among them, search for patterns and identify potential candidates for synthesis. We focus especially on new caged geometries, and our results indicate that the prismatic ones can be expected to present higher energy densities and be very stable with respect to unimolecular decomposition. It is shown that the energy content can be clearly stratified between chain, ring, cage and prismatic cage structures.

1 Introduction

Polynitrogen systems (polyN) have been the subject of a vast number of studies in the past decades, both in neutral and ionic forms, due to the fact that they are candidates for clean energy sources. This comes from the nature of their structures, built by single and/or double N–N bonds. The triple bond of molecular nitrogen is highly thermodynamically stable, and therefore these systems tend to decompose, dissociating into N_2 molecules and releasing large amounts of energy. As the product of this dissociation is the major component of atmospheric air, this process occurs without the formation of polluting compounds or greenhouse gases, such as carbon dioxide.[1–4]

Because of their high potential energy content, polyN are part of a group of substances called high energy density materials (HEDMs). For practical usage, the material must not only be able to release a large amount of energy on demand, but also must have a reasonable chemical stability in order to be

produced and stored. For polyN systems, this means a high dissociation energy coupled with a relatively high decomposition barrier.[1]

PolyN species can be sub-categorized in chain, ring or caged structures. The latter tend to show more single bonds between nitrogen atoms, and thus may be expected to release a larger amount of energy when several new triple N_2 bonds are formed upon its dissociation. As this process may involve the breaking of several chemical bonds simultaneously, its decomposition barrier is also expected to be higher.[5] Therefore, cage-like structures are possibly the most suitable ones for HEDM use.

Experimentally, it is very hard to synthesize polyN at ambient conditions. Usually, extremely high pressures and cryogenic temperatures are necessary.[6,7] In the field of neutral polyN, it has already been reported a covalent allotropic form of nitrogen in which the atoms are arranged in a cubic gauche structure (cg-N),[8] a polymeric nitrogen with the black phosphorus structure (bp-N)[9] and a molecular form of N_8.[10] On the ionic front, on the other hand, many species have been obtained over the past few years, such as the pentazolate anion,[11] the pentazenium cation[12,13] and metal pentazolate hydrate complexes.[14] Slightly larger anions have also been recently reported, such as a tungsten hexanitride[15] and the N_8^- anion, which has been synthesized on the sidewalls of multi-walled carbon nanotubes[16] and also stabilized on boron-doped graphene.[17]

Theoretically, several studies involving polyN (especially up to 10 atoms) have been reported over the past decades, regarding their structures and thermodynamic properties, both

[a]Centro Federal de Educação Tecnológica de Minas Gerais, CEFET-MG, Av. Amazonas 5253, (30421-169) Belo Horizonte, Minas Gerais, Brazil. E-mail: brenogalvao@gmail.com

[b]Programa de Pós-Graduação em Modelagem Matemática e Computacional, Centro Federal de Educação Tecnológica de Minas Gerais, CEFET-MG, Av. Amazonas 7675, (30510-000) Belo Horizonte, Minas Gerais, Brazil

† Electronic supplementary information (ESI) available: Structures and frequencies obtained at the M06-2X and SOGGA11-X/def2-TZVPP levels; graphs of selected molecular parameters against AE, DE and DE/*n*. See DOI: 10.1039/d1ra03259c

in neutral[18–36] and ionic forms at gas phase.[22,37–40] Stable molecular crystals of N_6, N_8 and N_{10} [2,41–43] have also been proposed. However, less attention has been given to their dissociation and isomerization barriers, which is a key aspect to predict what isomeric forms may actually be stable at ordinary temperatures, which is a major advantage for storage. Most of previous research that has been published on this property focused on chain or ring structures with up to 10 atoms for neutral[4,6,7,44–60] and ionic forms.[7,52,54,59,61–65] To the best of our knowledge, the dissociation and isomerization barriers of neutral caged structures have been, up until now, little exploited,[66–69] and most of these studies employed symmetry constraints in the search for transition state structures.

For the reasons mentioned above, this work is focused on providing a systematic study on the decomposition mechanisms for several polyN neutral molecules, in order to provide insights into what type of structure might be best suitable for HEDMs. The various isomers are compared by their calculated dissociation barriers and dissociation energies using the same theoretical level for all structures and without symmetry constraints in the decomposition pathways, allowing for a fair comparison between all structures. We focus on caged geometries, but for each polyN size, other relevant structures are always included for a direct analysis between the different classes.

2 Methodology

All electronic structure calculations reported here were performed using the GAMESS-US[70] and MOLPRO[71] packages. The calculations were based on density functional theory (DFT)[72] using the def2 (SVP and TZVPP) basis sets.[73] The M06-2X[74] and SOGGA11-X[75,76] exchange and correlation functionals were chosen due to their known accuracy for predicting energy barrier heights.[77,78] In fact, it has been shown by Peverati and Truhlar,[76] that the mean unsigned error (MUE) for non-hydrogen-transfer barrier heights (NHTBH) for the hybrid SOGGA11-X functional and of M06-2X are respectively 1.16 kcal mol^{-1} and 1.22 kcal mol^{-1}. Therefore both functionals show chemical accuracy for potential energy barriers and are expected to provide reliable results for our purposes. Vibrational analysis was carried out to confirm the minima and transition states (TSs) found within the employed levels of theory. The wxMacMolPlt program was used for graphic visualization and representation of the molecular geometries.[79]

The initial structures selected (shown in Fig. 1) were taken from ref. 36 and 80 and were chosen such as to provide four different structures for each molecular size, and to present a diverse set of all geometrical classes of structures. This work provides the first account on the unconstrained dissociation paths of six nitrogen allotropic forms: $N_8(C_{2v})$-A, $N_8(C_S)$, and all four N_{10} isomers including the prismatic one.

As a first step, the smaller def2-SVP basis set was used for an initial exploration of possible dissociation and isomerization paths associated with each studied polyN. Intrinsic reaction coordinate (IRC) calculations were performed with this basis set using the Gonzalez–Schlegel second-order algorithm[81] for all
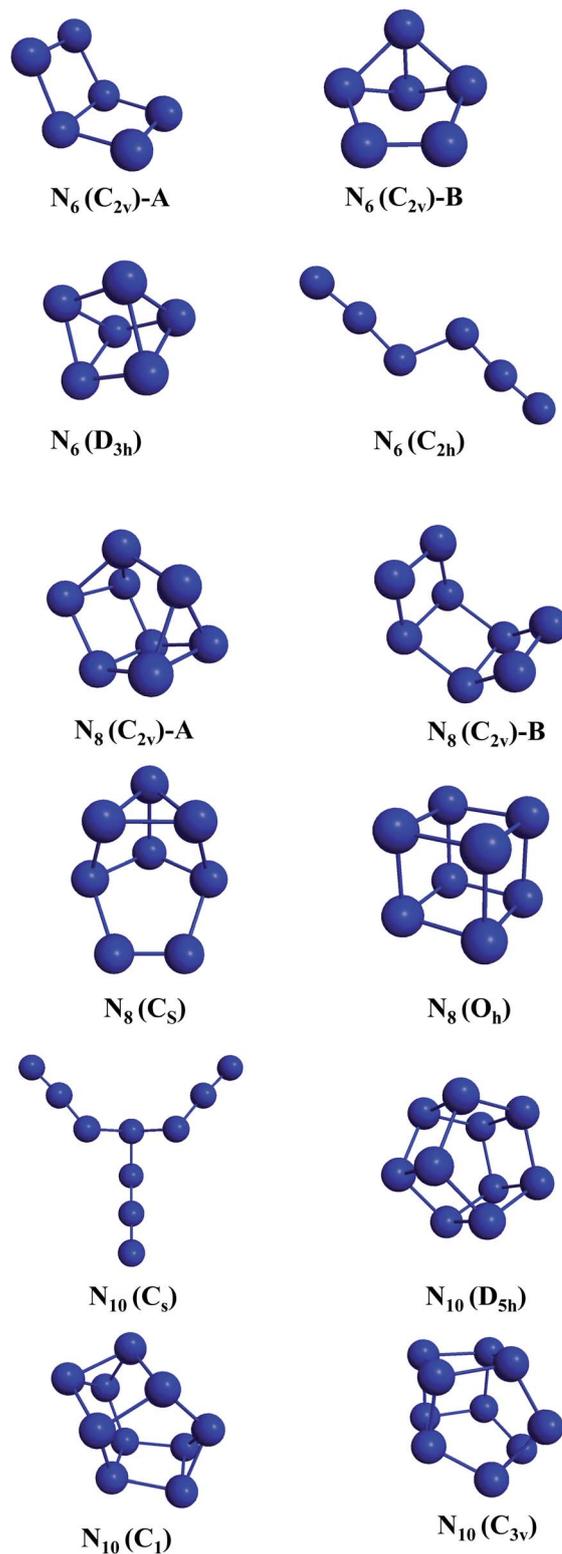

Fig. 1 Initial structures.

TSs found to ensure their connection to decomposition or isomerization products. After that, reoptimization employing the larger def2-TZVPP basis set was carried out for all stationary points found. The energies of all minima and TSs were zero-

point energy (ZPE) corrected within the def2-TZVPP approach and no symmetry restrictions were imposed in any case.

To assess the performance of our DFT results, we have also performed geometry optimizations and frequencies calculations at the coupled cluster singles and doubles and perturbative triples (CCSD(T)) level,[82–84] using the cc-pVDZ basis set.[85,86] This was followed by a single point energy refinement using the explicitly correlated coupled cluster method (CCSD(T)-F12) method,[87,88] using the aug-cc-pVTZ basis set. Such calculations were considered as benchmark and the results were directly compared to the DFT ones.

3 Results

In the results presented throughout this work, the energies in all graphs are given relatively to the nN_2 dissociation limit. The reaction pathways in the IRC plots are displayed with black circles (at the SOGGA11-X/def2-SVP level). The horizontal lines in these graphs correspond to the ZPE corrected energies at M06-2X/def2-TZVPP (orange) and SOGGA11-X/def2-TZVPP (black) levels.

For a summary of the results, the tables in this section show the numerical values of the activation energy (AE) and dissociation energies (DE), which are positively defined as

$$AE = E_{TS} + ZPE_{TS} - [E_{polyN} + ZPE_{polyN}] \quad (1)$$

and

$$DE = E_{polyN} + ZPE_{polyN} - \frac{n}{2}[E_{N_2} + ZPE_{N_2}] \quad (2)$$

where E_{TS}, E_{polyN} and E_{N_2} stand for the total energies of the transition state, the initial polyN and a nitrogen molecule, respectively. ZPE_{TS}, ZPE_{polyN} and ZPE_{N_2} are the corresponding zero-point energies of these species and n is the total number of atoms of the polyN. In the calculation of AE, only the lowest lying TS is considered. In summary, AE is a measure of how
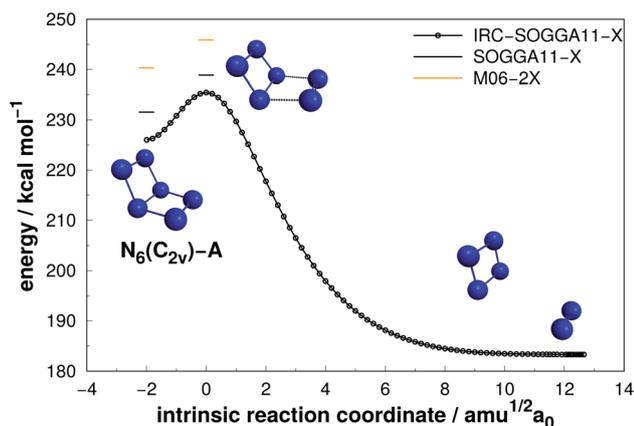

Fig. 3 Decomposition path of $N_6(C_{2v})$-B isomer with IRC calculation following the scheme of Fig. 2.

difficult it is to break the polyN structure in an unimolecular decomposition, while DE gives the amount of energy released in the process. We also report the values of dissociation energy per atom (DE/n), since this is more related to the energy content of the HEDM.

The Cartesian coordinates and frequencies of all minima and transition states reported in this section are given in the ESI† for both DFT functionals. Although the results of both functionals are given in the figures and tables, the energies discussed in the text are given only at the SOGGA11-X/def2-TZVPP level for simplicity.

3.1 N_6

Four isomers of N_6 have been considered in the present work. Fig. 2–5 present the results of the IRC calculations for structures $N_6(C_{2v})$-A, $N_6(C_{2v})$-B, $N_6(C_{2h})$ and $N_6(D_{3h})$ respectively. Table 1 gathers their AE and DE values. All three different calculation methods predict the same energetic ordering between the four structures, and both DFT functionals are in fairly good agreement with the CCSD(T)-F12/aug-cc-pVTZ//CCSD(T)/cc-pVDZ

Fig. 2 Decomposition path of $N_6(C_{2v})$-A isomer obtained from IRC calculation at SOGGA11-X/def2-SVP level. The bars correspond to the zero-point corrected energies at M06-2X/def2-TZVPP (orange) and SOGGA11-X/def2-TZVPP (black) levels. The zero of energy is set as the fully dissociated system (nN_2).

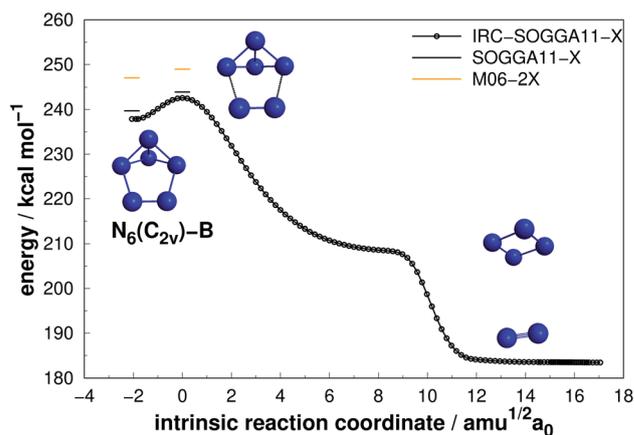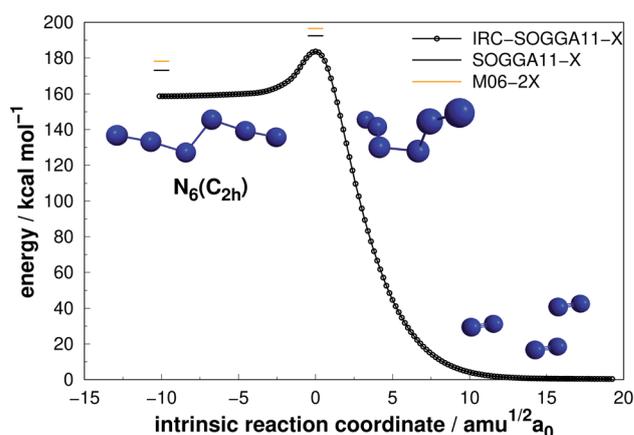**Fig. 4** Decomposition path of $N_6(C_{2h})$ isomer obtained from IRC calculation following the scheme of Fig. 2.
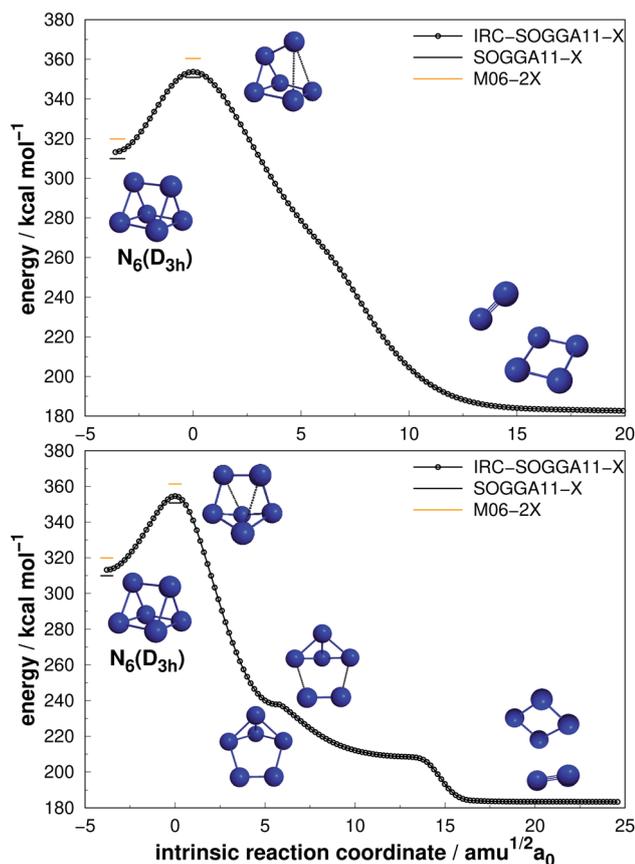
Fig. 5 Direct decomposition path of $N_6(D_{3h})$ isomer into $N_4(D_{2h})$ + N_2 (upper panel) and an alternative path to the same products passing through an intermediate (lower panel). Following the scheme of Fig. 2.
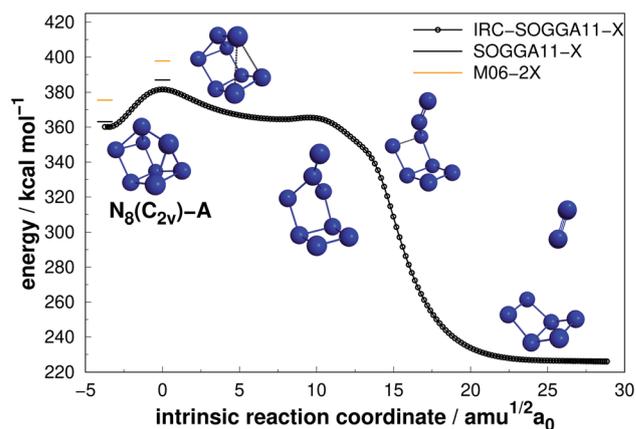

Fig. 6 Decomposition path of $N_8(C_{2v})$-A isomer obtained from IRC calculation following the scheme of Fig. 2.

regarding which structure is more stable towards unimolecular decomposition. A broader comparison between the methods and their accuracy will be given in the discussion section.

As it can be seen, isomers $N_6(C_{2v})$-A (which shows a Dewar benzene structure) and $N_6(C_{2v})$-B possess small dissociation barriers (AE of 7.33 and 4.23 kcal mol^{-1}, respectively), indicating that they are kinetically unstable at ambient conditions. These isomers decompose in a stepwise process, being the first the elimination of a N_2 molecule, followed by the dissociation of the well known D_{2h} form of N_4,[7,58] which has a very small dissociation barrier (around 6.45 kcal mol^{-1} above the N_4 well[7]).

The $N_6(C_{2h})$ isomer, also named as diazide, presents a considerably higher decomposition barrier (19.23 kcal mol^{-1}) when compared to the previous two, in spite of its chain configuration. Nevertheless, it may not be sufficient to confirm its stability at room temperature, as it has been suggested that an energy barrier of approximately 30 kcal mol^{-1} is desirable.[50,67] In agreement with previous studies,[48,52,60,67] we found a concerted dissociation mechanism in which $N_6(C_{2h})$ breaks directly into three N_2 molecules. It is worth mentioning that Greschner et al.[41] recently predicted a stable molecular crystal

results for DE. The mean absolute difference between the benchmark results and the M06-2X one is only 2.0%, with a standard error of the mean (SEM) of 0.2%. A similar comparison is obtained for the SOGGA11-X functional, with a mean absolute difference of 2.2%. This good agreement between the methods reinforces the conclusions of this work

Table 1 Activation energy barriers (AE), dissociation energies (DE) and dissociation energies per nitrogen atoms (DE/n) in kcal mol^{-1} for the N_6 isomers

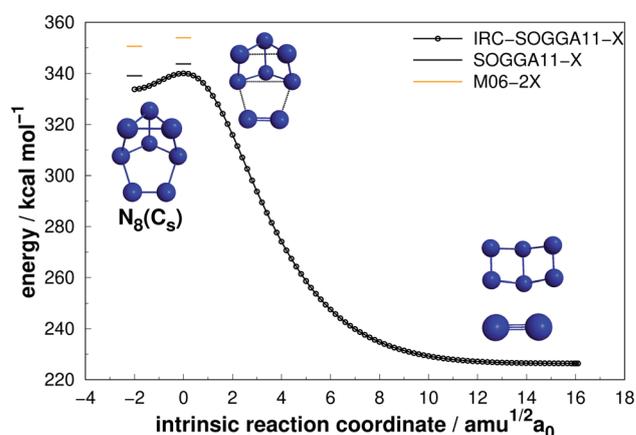| Structure	Method	AE	DE	DE/n
$N_6(C_{2v})$-A	M06-2X	5.59	240.30	40.05
	SOGGA11-X	7.33	231.53	38.59
	CCSD(T)-F12		235.12	39.19
	M06-2X	1.94	247.00	41.17
$N_6(C_{2v})$-B	SOGGA11-X	4.23	239.69	39.95
	CCSD(T)-F12		243.65	40.61
	M06-2X	18.42	178.13	29.69
$N_6(C_{2h})$	SOGGA11-X	19.23	173.20	28.87
	CCSD(T)-F12		181.77	30.29
	M06-2X	40.53	319.89	53.32
$N_6(D_{3h})$	SOGGA11-X	40.96	309.90	51.65
	CCSD(T)-F12		312.61	52.10

Fig. 7 Decomposition path of $N_8(C_s)$ isomer obtained from IRC calculation following the scheme of Fig. 2.
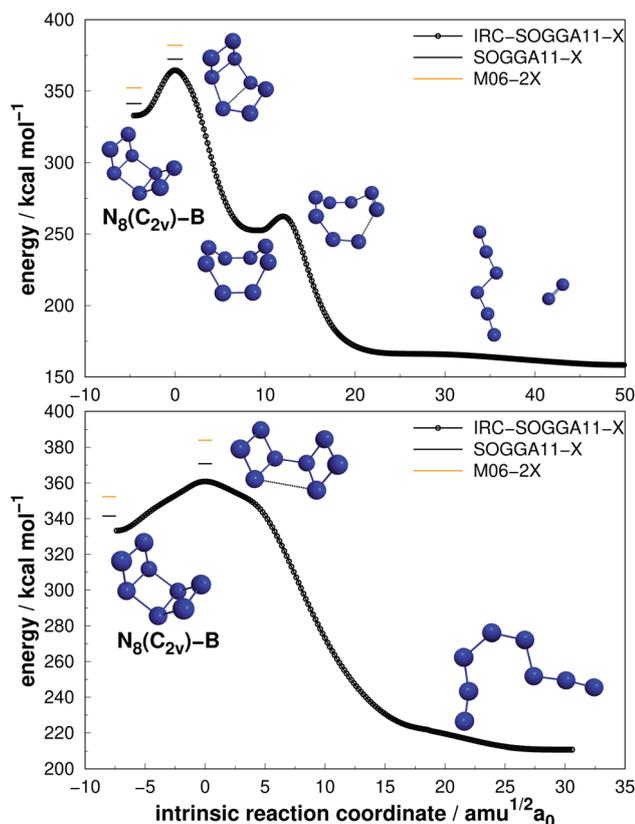
Fig. 8 The two possible paths for $N_8(C_{2v})$-B with energetically equivalent barriers as indicated in the text. Following the scheme of Fig. 2.

composed of $N_6(C_{2h})$ chains. Their molecular dynamics simulations suggest reasonable thermal stability.

Differently from the other three, $N_6(D_{3h})$ (or prismane) shows more promising results. In our study, we found a new TS that connects prismane directly to $N_4(D_{2h})$ + N_2, with an energy barrier of 40.96 kcal mol^{-1} (upper panel in Fig. 5). Li and Liu[67] found instead a considerable isomerization energy barrier

towards the $N_6(C_{2v})$-B structure (34.4 kcal mol^{-1}) at CCSD/6-311G(d)(energies)//B3LYP/6-311G(d)(geometries) level. We could also find the isomerization path connecting these two isomers (lower panel in Fig. 5), and an energy barrier of 40.84 kcal mol^{-1} was obtained. Within the accuracy of our calculations, both isomerization and dissociation processes can be considered as energetically equivalent. The $N_6(C_{2v})$-B isomer, in turn, will easily dissociate as illustrated in Fig. 3. These barriers are a good indicative of practical use of $N_6(D_{3h})$ as HEDM, and the unraveling of the direct decomposition pathway is relevant to the understanding of the energy landscape associated with prismane.

Within the N_6 size, prismane releases the largest amount of energy considering its dissociation into three N_2 molecules, being 78% more exothermic than the chain isomer ($N_6(C_{2h})$). Its AE is also more than two times higher than that of $N_6(C_{2h})$, indicating that it may be stable on higher temperatures. This can be partially attributed to its caged geometry, but as will be explored later in section 4, not all caged structures follow this pattern, and there are other features involved.

3.2 N_8

Four allotropes of N_8 have been considered in the present work. Fig. 6–9 present the results of the IRC calculations for isomers $N_8(C_{2v})$-A, $N_8(C_s)$, $N_8(C_{2v})$-B and $N_8(O_h)$, respectively. To the best of our knowledge, this is the first work regarding the dissociation barriers of $N_8(C_{2v})$-A and $N_8(C_s)$. Table 2 presents the values of their AEs and DEs. It should be noted that azidopentazole has been found to be the lowest energy isomer of N_8, but ref. 49 and 50 already ruled out the possibility that this could be a good candidate for a HEDM.

Regarding the $N_8(C_{2v})$-A isomer, we found a decomposition path that leads to $N_6(C_{2v})$-A + N_2 (Fig. 6). It passes through an intermediate resulting from the opening of a triangular ring of the initial structure. The isomerization barrier that is determinant to the decomposition process was found to be 23.72 kcal mol^{-1} (AE). Although not as high as that of prismane, this isomer might be an interesting candidate for production.

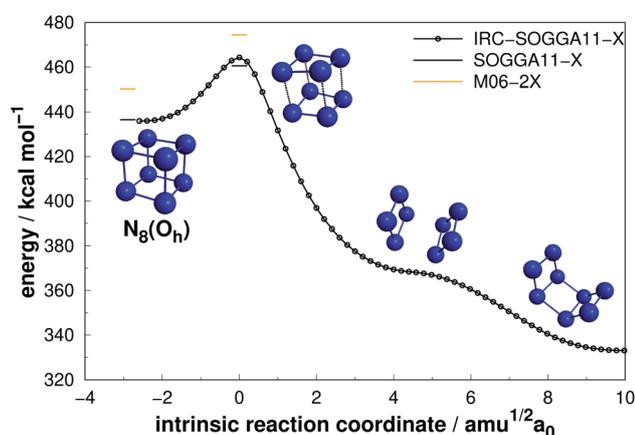**Fig. 9** Isomerization path of $N_8(O_h)$ into $N_8(C_{2v})$-B. Following the scheme of Fig. 2.

Table 2 Activation energy barriers (AE), dissociation energies (DE) and dissociation energies per nitrogen atoms (DE/n) in kcal mol^{-1} for the N_8 isomers

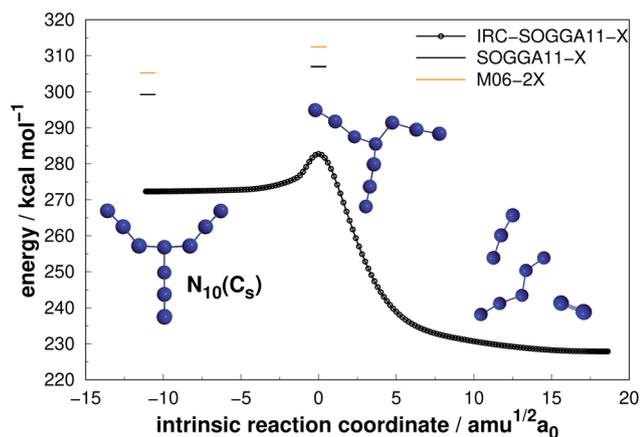| Structure	Method	AE	DE	DE/n
$N_8(C_{2v})$-A	M06-2X	22.26	375.47	46.93
	SOGGA11-X	23.72	363.13	45.39
	CCSD(T)-F12		367.69	45.96
	M06-2X	31.65	352.27	44.03
$N_8(C_{2v})$-B	SOGGA11-X	29.34	341.44	42.68
	CCSD(T)-F12		344.10	43.01
	M06-2X	3.33	350.60	43.83
$N_8(C_s)$	SOGGA11-X	4.53	339.09	42.39
	CCSD(T)-F12		341.98	42.75
	M06-2X	24.11	450.31	56.29
$N_8(O_h)$	SOGGA11-X	24.06	436.51	54.56
	CCSD(T)-F12		435.88	54.49

Fig. 10 Decomposition path of $N_{10}(C_s)$ isomer obtained from IRC calculation following the scheme of Fig. 2.

On the other hand, the $N_8(C_s)$ isomer did not present promising results, as its predicted barrier for decomposition into $N_6(C_{2v})$-A $+ N_2$ is only 4.53 kcal mol^{-1} (see Fig. 7).

More interesting results were achieved for the $N_8(C_{2v})$-B isomer within our calculations. At the preliminary exploration using the def2-SVP basis set, only one barrier was found to be relevant. However, when we reoptimized the minima and TSs using the def2-TZVPP basis set, another barrier presented a similar and promising result, and we report both. First, a mechanism that leads to a D_{2d} structure followed by decomposition to $N_6(C_{2h}) + N_2$ with an activation energy of 30.84 kcal mol^{-1} (upper panel in Fig. 8). Second, a direct decomposition route through a structure opening transition state yielded an activation energy of 29.34 kcal mol^{-1}, leading to an open chain $N_8(C_1)$ isomer (lower panel in Fig. 8). Both barriers are high and show similar values, and thus $N_8(C_{2v})$-B may be another relevant candidate. Fau and Bartlett[62] reported that isolated open chains of N_8 possess a relatively low decomposition barrier. In their work, this C_1 structure is easily decomposed to $N_6 + N_2$.[62]

Still regarding $N_8(C_{2v})$-B, it should be noted that a TS directly connecting it to full dissociation, was obtained by Schmidt *et al.*[68] at the MP2/6-31G(d) level, with an AE of 20 kcal mol^{-1}, but could not be reproduced within our calculation method. Gagliardi *et al.*[66] found (employing B3LYP/cc-pVTZ calculations) two pathways for this structure: one similar to that shown in the upper panel of Fig. 8, with a barrier of 43.3 kcal mol^{-1}, and another for isomerization of $N_8(C_{2v})$-B into another structure of 28.2 kcal mol^{-1}. In summary, the final AE value reported in ref. 66 is similar to the one reported here.

Extensive research has been performed on the octaazacubane allotrope,[6,44,47,66,68,69] $N_8(O_h)$. Engelke and Stine[44] studied the concerted symmetry forbidden D_{4h} dissociation path $N_8(O_h) \rightarrow 4N_2$ and found a 162 kcal mol^{-1} energy barrier at RHF/4-31G* level, in good agreement with the work of Evangelisti and Gagliardi[47] (159 kcal mol^{-1} at CASSCF/VDZP level) considering the same constrained D_{4h} path. However, both studies agree that octaazacubane dissociation should occur in a less symmetric path. On the other hand, an almost barrierless pathway to the total decomposition of the isolated $N_8(O_h)$ into $4N_2$ (2.5 kcal mol^{-1}) was obtained by Gimaldinova *et al.* within the frame of the non-orthogonal tight-binding model for describing interatomic interactions.[6]

The lowest energy TS linked to $N_8(O_h)$ that we managed to find in the present study lies 24.06 kcal mol^{-1} above it. According to our IRC calculations, this TS actually connects $N_8(O_h)$ to the $N_8(C_{2v})$-B isomer. Our proposed isomerization pathway agrees with the results of ref. 66, 68 and 89. After isomerization, $N_8(O_h)$ may readily follow the $N_8(C_{2v})$-B decomposition path already discussed and presented in Fig. 8. Therefore, analogously to the $N_8(C_{2v})$-B isomer, octaazacubane may also be of experimental relevance, but with the advantage of generating 28% more energy upon full dissociation.

Octaazacubane, $N_8(O_h)$, presents the highest DE/n ratio among all polyN studied here, which can be attributed to its strained prismatic structure where each N atom makes 3 single bonds. On the other hand, our calculations show that $N_8(C_{2v})$-B (which does not show a caged structure) shows the highest activation energy for the 8 atoms polyN. As will be summarized
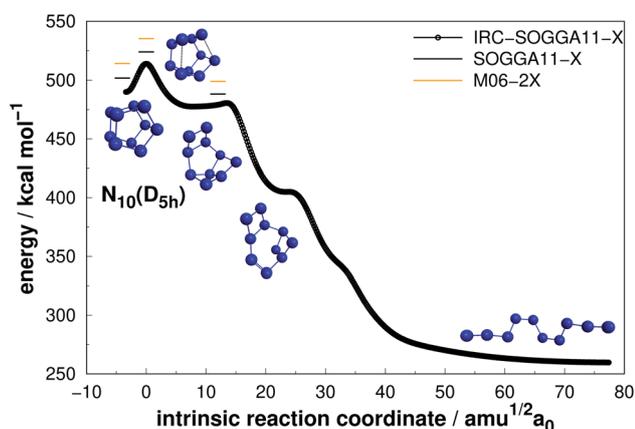

Fig. 11 Decomposition path of $N_{10}(D_{5h})$ isomer obtained from IRC calculation following the scheme of Fig. 2.
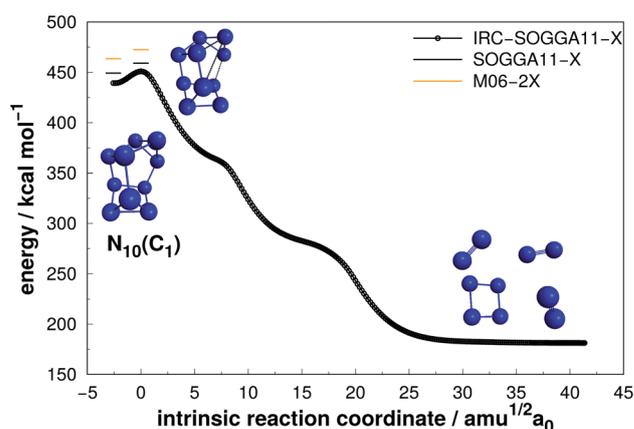

Fig. 12 Decomposition path of $N_{10}(C_1)$ isomer obtained from IRC calculation following the scheme of Fig. 2.
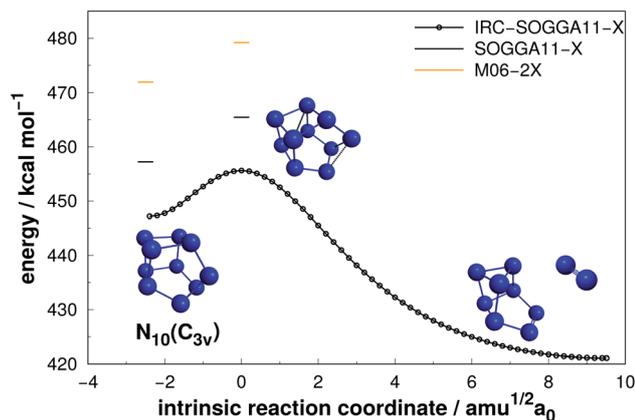
Fig. 13 Decomposition path of $N_{10}(C_{3v})$ isomer obtained from IRC calculation following the scheme of Fig. 2.

later, although it is possible to draw correlations between the geometric shape and DE values, a similar analysis often fails to explain the calculated AEs. Finally, the relatively small difference between the dissociation barriers of $N_8(C_{2v})$-B and $N_8(O_h)$ (5.3 kcal mol^{-1}) compared to the significant difference between their DEs (95 kcal mol^{-1}) should be taken into consideration.

3.3 N_{10}

Four allotropes of N_{10} have been considered in the present work. Fig. 10–13 present the results of the IRC calculations for isomers $N_{10}(C_s)$, $N_{10}(D_{5h})$, $N_{10}(C_1)$ and $N_{10}(C_{3v})$, respectively. To the best of our knowledge, this is the first work to provide fully relaxed dissociation mechanisms for these structures. The numerical results are gathered in Table 3. The difference between the two exchange correlation functionals employed in the case of the N_{10} structures follows the same trend observed for the previous structures: both functionals predict very similar AE barriers, but M06-2X predicts larger DEs.

The branched chain isomer $N_{10}(C_s)$ possesses a small decomposition barrier 7.73 kcal mol^{-1} and may not be a good candidate for HEDM. Together with the other chain isomer

explored in this work ($N_6(C_{2h})$), they represent the lowest DE/n ratio. Interestingly, $N_6(C_{2h})$ has a decomposition barrier 2.5 times larger than $N_{10}(C_s)$, despite the analogous structures, which again indicates the difficulty in correlating the AE value with molecular shape.

The prismatic $N_{10}(D_{5h})$ isomer decomposes in a stepwise fashion, passing through two different intermediates, to reach a chain isomer (Fig. 11). As reported by Strout,[55] such acyclic forms of N_{10} tend to present low activation barriers towards dissociation, and thus the system will easily dissociate from there. Therefore, if there is available energy for $N_{10}(D_{5h})$ to surpass the first isomerization barrier (25.81 kcal mol^{-1}), it will promptly undergo dissociation. This barrier is comparable to those presented by $N_8(C_{2v})$-B and $N_8(O_h)$ isomers which, together with a large energy released upon full dissociation (DE), makes $N_{10}(D_{5h})$ the most attractive polyN within the N_{10} structures according to our calculations. The just published study employing reaction dynamics[89] obtained a similar transition state, but the B3LYP reported energy barrier is substantially lower (13 kcal mol^{-1}). Since the B3LYP functional is well known to underestimate barrier heights,[90,91] with a MUE about four times higher than the functionals employed here,[76] our AE value should be more realistic.

Even though $N_{10}(C_1)$ and $N_{10}(C_{3v})$ present cage-like structures and high energy content (as given by DE/n), their rather small decomposition energy barriers (AE) make them not suitable for HEDM application. This is also the case for smaller polyN such as $N_8(C_s)$ and $N_6(C_{2v})$-B, although all of them present significant DEs. Therefore, despite caged structures are consistently related to higher DEs, this is not the main factor governing their decomposition barriers. Symmetry seems to play an important role, as specific prismatic structures with peripheral $N_4(D_{2h})$ rings tended to yield higher kinetic stability, as well as DEs. Like the other prismatic structures of smaller nuclearities approached here, $N_{10}(D_{5h})$ is the isomer that releases the greatest amount of energy towards full decomposition into N_2 molecules.

4 Discussion

For summarizing the results we first present a graph based on the Evans–Polanyi principle,[92] relating activation energy with reaction energy, which is shown in Fig. 14. Although no clear correlation between AE and DE is observed, this graph is helpful for a general overview. First of all, the two graphs show that both functionals (one hybrid-GGA and one of meta-GGA type), are in very good agreement and the exact same conclusions can be drawn from both. In fact, analysing all structures calculated in this work, the difference between the two functionals in predicting DE is on average 3.1%, with a SEM of 0.1%. The SOGGA11-X functional is in better agreement with the benchmark calculations, in average deviating from the CCSD(T)-F12 ones by only 1.5% with a SEM of 0.4%. As for the AE values, the two funcionals always agree qualitatively in predicting the order of increasing AE. The difference between their calculated AEs is on average 1.19 kcal mol^{-1} which is indeed their expected accuracy.

Table 3 Activation energy barriers (AE), dissociation energies (DE) and dissociation energies per nitrogen atoms (DE/n) in kcal mol^{-1} for the N_{10} isomers

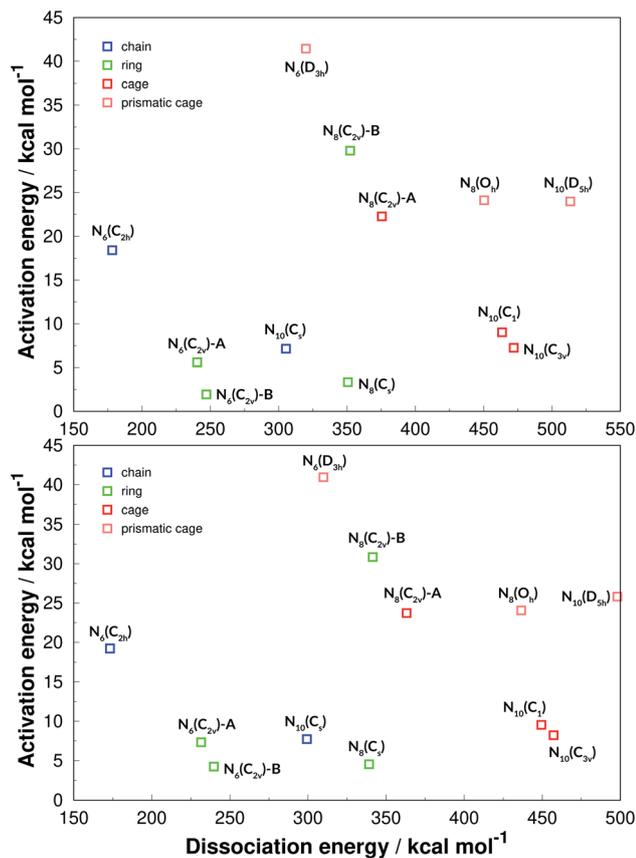| Structure	Method	AE	DE	DE/n
$N_{10}(C_s)$	M06-2X	7.14	305.30	30.53
	SOGGA11-X	7.73	299.23	29.92
	CCSD(T)-F12		312.74	31.27
	M06-2X	23.97	513.39	51.34
$N_{10}(D_{5h})$	SOGGA11-X	25.81	498.12	49.81
	CCSD(T)-F12		499.31	49.93
	M06-2X	9.02	463.42	46.34
$N_{10}(C_1)$	SOGGA11-X	9.55	449.47	44.95
	CCSD(T)-F12		454.18	45.42
	M06-2X	7.24	471.95	47.19
$N_{10}(C_{3v})$	SOGGA11-X	8.22	457.24	45.72
	CCSD(T)-F12		459.62	45.96

Fig. 14 Evans–Polanyi plot. The results of the M06-2X functional are given in the upper panel, while SOGGA11-X ones are in the lower panel.

We have also classified the structures into chains, rings, cages and caged prisms, which is presented in Fig. 14 in different colors. It is clearly seen that prismatic structures always show large activation energies towards unimolecular decomposition, and that of prismane $N_6(D_{3h})$ is specially high. This plot is helpful for an easy visualization of polyN molecules that display high values for both AE and DE, and thus could be good candidates for HEDMs. Besides the prismatic structures, $N_8(C_{2v})$-B shows a surprisingly high activation energy, and could be one of the best candidates explored here. The chain structure of $N_6(C_{2h})$ shows a significant decomposition barrier, even though it is the structure that releases the least amount of energy upon dissociation into nitrogen molecules. It is worth recalling that Greschner et al.[41] proposed a stable molecular crystal composed of $N_6(C_{2h})$ chains.

Although we have shown that all prismatic structures show high activation energies, it is seen that having a caged structure is not a sufficient condition. All caged structures present a high energy content (DE) but for some reason it is relatively easy to break some of them (small AE). Ring structures often have low activation energy, and are easier to break but, as seen before, $N_8(C_{2v})$-B is an exception.

For a global analysis of all results given in the previous section, and also aiming to find correlations between the energetic properties with electronic and structural ones, we have calculated several molecular parameters such as HOMO–LUMO gap, average bond order, average bond length and asphericity for all polyN structures reported here. After the calculations we plotted these properties against AE, DE and DE/n, which are all given in the ESI† for both DFT functionals.

None of the molecular parameters explored here were found to correlate with AE. If such correlation existed, it would be very useful for predicting the dissociation barriers of new polyN structures obtained in the future, since exploring their high dimensional PES in the search for the lowest TS is a very difficult task.

The average bond lengths and average bond orders were found to be correlated with DE and DE/n. The latter is shown in Fig. 15, where it is seen that lower bond orders (and higher bond lengths, as given in the ESI†) generally mean higher dissociation energy. It is interesting to see that DE/n, which is more related to the energy content of a structure than DE, can be clearly stratified among the four geometrical categories (chain, ring, cage and caged prism), which was not observed in the case of DE (see Fig. 14). Although caged prisms have higher DE/n than caged structures, their average bond orders are similar, lying below 0.9. Ring structures have average bond
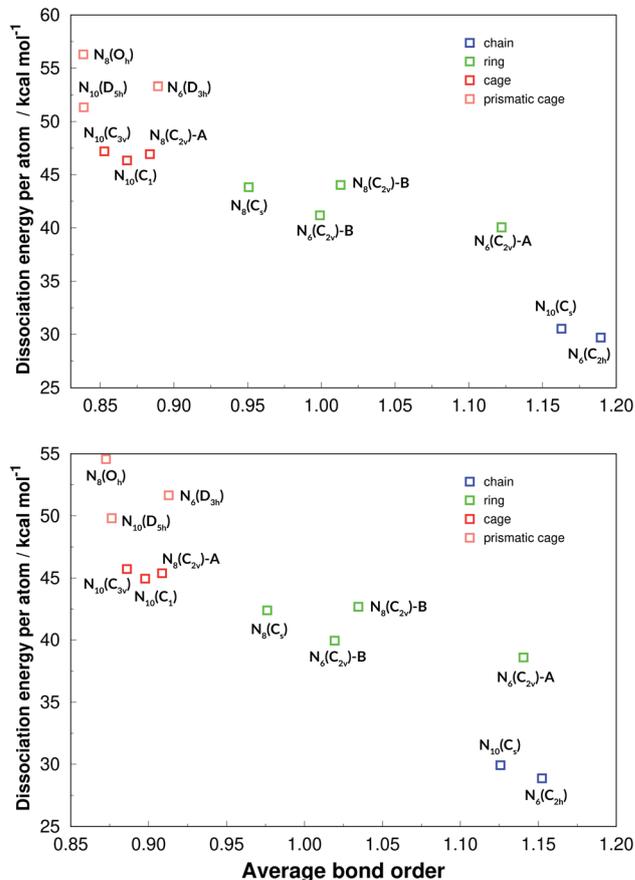

Fig. 15 Dissociation energies per nitrogen atoms in function of the average bond orders. Results at the def2-TZVPP level of theory. M06-2X (upper panel) and SOGGA11-X (lower panel).

orders from 0.95 to 1.14, while chained structures show the largest values, as more double bonds are possible.

5 Conclusions

In this work, the unimolecular decomposition routes for several polynitrogen allotropes were predicted at the SOGGA11-X/def2-TZVPP and M06-2X/def2-TZVPP levels of theory. These two methods were shown to yield similar results, compare well with highly accurate CCSD(T)-F12 ones, and the same conclusions can be drawn from both.

Though the potential barriers for some polyN have been previously explored in the literature, this work provides new accounts on the unconstrained decomposition of six structures: $N_8(C_{2v})$-A, $N_8(C_s)$, and all four N_{10} isomers, including the prismatic one. Furthermore, new mechanisms involving prismane and $N_8(C_{2v})$-B were obtained.

By using the same computational methods for three different sizes, and several geometrical shapes for each, we were able to extract interesting information about this class of chemical systems. First, it is shown that the energy content (DE/n, which may be released if these substances are used as energy sources) can be clearly stratified between chain, ring, cage and prismatic cage structures. This variable shows a linear correlation with average bond size and average bond order.

The energy barriers towards unimolecular decomposition (AE) could not be correlated to any electronic or geometrical property of the molecule. If such correlation existed, it would be very useful for screening newly proposed polyN structures, as the search for the dissociation transition states is a very time consuming task.

Comparing between individual structures, it is found that prismane ($N_6(D_{3h})$) shows a very high dissociation barrier and, if it could be synthesized, would be very stable, perhaps allowing its storage at ambient conditions. Upon triggering its dissociation reaction, it would deliver a very large amount of energy, without producing any pollutant products.

All prismatic cage structures are shown to have considerably high activation energies as well. Although $N_8(O_h)$ and $N_{10}(D_{5h})$ do not display an AE as high as that of prismane, they also have a very large energy content. An unexpected promising case was $N_8(C_{2v})$, a boat-like structure that displays an activation energy even higher than those of the $N_8(O_h)$ and $N_{10}(D_{5h})$ prismatic structures.

The present overall survey of possible polyN structures may serve as a guide for future computational work, to direct efforts in finding crystal structures and other properties only for the most promising and kinetically stable polyN structures.

Conflicts of interest

There are no conflicts of interest to declare.

Acknowledgements

References

1 P. C. Samartzis and A. M. Wodtke, All-nitrogen chemistry: how far are we from N_{60}?, *Int. Rev. Phys. Chem.*, 2006, **25**, 527–552.

2 B. Hirshberg, R. B. Gerber and A. I. Krylov, Calculations predict a stable molecular crystal of N_8, *Nat. Chem.*, 2014, **6**, 52–56.

3 V. Zarko, Searching for ways to create energetic materials based on polynitrogen compounds, *Combust., Explos. Shock Waves (Engl. Transl.)*, 2010, **46**, 121–131.

4 M. R. Manaa, Toward new energy-rich molecular systems: from N_{10} to N_{60}, *Chem. Phys. Lett.*, 2000, **331**, 262–268.

5 T. Brinck and M. Rahm, Theoretical Design of Green Energetic Materials: Predicting Stability, Detection, Synthesis and Performance, in *Green Energetic Materials*, John Wiley & Sons, Chichester, UK, 2014.

6 M. A. Gimaldinova, K. P. Katin, K. S. Grishakov and M. M. Maslov, Kinetic stability of nitrogen cubane inside the fullerene cage: Molecular dynamics study, *Fullerenes, Nanotubes, Carbon Nanostruct.*, 2020, **28**, 304–308.

7 M. T. Nguyen, Polynitrogen compounds: 1. Structure and stability of N_4 and N_5 systems, *Coord. Chem. Rev.*, 2003, **244**, 93–113.

8 M. I. Eremets, A. G. Gavriliuk, I. A. Trojan, D. A. Dzivenko and R. Boehler, Single-bonded cubic form of nitrogen, *Nat. Mater.*, 2004, **3**, 558–563.

9 D. Laniel, B. Winkler, T. Fedotenko, A. Pakhomova, S. Chariton, V. Milman, V. Prakapenka, L. Dubrovinsky and N. Dubrovinskaia, High-pressure polymeric nitrogen allotrope with the black phosphorus structure, *Phys. Rev. Lett.*, 2020, **124**, 216001.

10 S. Duwal, Y.-J. Ryu, M. Kim, C.-S. Yoo, S. Bang, K. Kim and N. H. Hur, Transformation of hydrazinium azide to molecular N_8 at 40 GPa, *J. Chem. Phys.*, 2018, **148**, 134310.

11 C. Zhang, C. Sun, B. Hu, C. Yu and M. Lu, Synthesis and characterization of the pentazolate anion cyclo-N5 in $(N_5)_6(H_3O)_3(NH_4)_4Cl$, *Science*, 2017, **355**, 374–376.

12 K. O. Christe, D. A. Dixon, D. McLemore, W. W. Wilson, J. A. Sheehy and J. A. Boatz, On a quantitative scale for Lewis acidity and recent progress in polynitrogen chemistry, *J. Fluorine Chem.*, 2000, **101**, 151–153.

13 K. O. Christe, W. W. Wilson, J. A. Sheehy and J. A. Boatz, N_5^+: a novel homoleptic polynitrogen ion as a high energy density material, *Angew. Chem.*, 2001, **40**, 2947.

14 Y. Xu, Q. Wang, C. Shen, Q. Lin, P. Wang and M. Lu, A series of energetic metal pentazolate hydrates, *Nature*, 2017, **549**, 78–81.

15 N. P. Salke, K. Xia, S. Fu, Y. Zhang, E. Greenberg, V. B. Prakapenka, J. Liu, J. Sun and J.-F. Lin, Tungsten

Hexanitride with Single-Bonded Armchairlike Hexazine Structure at High Pressure, *Phys. Rev. Lett.*, 2021, **126**, 065702.

16 Z. Wu, E. M. Benchafia, Z. Iqbal and X. Wang, N_8^- polynitrogen stabilized on multi-wall carbon nanotubes for oxygen-reduction reactions at ambient conditions, *Angew. Chem.*, 2014, **126**, 12763–12767.

17 Z. Yao, M. Hu, Z. Iqbal and X. Wang, N_8^--Polynitrogen Stabilized on Boron-Doped Graphene as Metal-Free Electrocatalysts for Oxygen Reduction Reaction, *ACS Catal.*, 2019, **10**, 160–167.

18 W. J. Lauderdale, J. F. Stanton and R. J. Bartlett, Stability and energetics of metastable molecules: tetraazatetrahedrane (N_4), hexaazabenzene (N_6), and octaazacubane (N_8), *J. Phys. Chem.*, 1992, **96**, 1173–1178.

19 M. N. Glukhovtsev and P. von Ragué Schleyer, Structures, bonding and energies of N_6 isomers, *Chem. Phys. Lett.*, 1992, **198**, 547–554.

20 R. Engelke, *Ab initio* correlated calculations of six nitrogen (N_6) isomers, *J. Phys. Chem.*, 1992, **96**, 10789–10792.

21 M. L. Leininger, C. D. Sherrill and H. F. I. Schaefer, N_8: a structure analogous to pentalene, and other high-energy density minima, *J. Phys. Chem.*, 1995, **99**, 2324–2328.

22 M. N. Glukhovtsev, H. Jiao and P. v. R. Schleyer, Besides N_2, what is the most stable molecule composed only of nitrogen atoms?, *Inorg. Chem.*, 1996, **35**, 7124–7133.

23 B. M. Gimarc and M. Zhao, Strain energies in homoatomic nitrogen clusters N_4, N_6, and N_8, *Inorg. Chem.*, 1996, **35**, 3289–3297.

24 A. Tian, F. Ding, L. Zhang, Y. Xie and H. F. Schaefer, New isomers of N_8 without double bonds, *J. Phys. Chem. A*, 1997, **101**, 1946–1950.

25 L. Gagliardi, S. Evangelisti, B. O. Roos and P.-O. Widmark, A theoretical study of ten N_8 isomers, *J. Mol. Struct.*, 1998, **428**, 1–8.

26 C. Chen, K.-C. Sun and S.-F. Shyu, Theoretical study of various N_{10} structures, *J. Mol. Struct.*, 1999, **459**, 113–122.

27 C. Chen and S.-F. Shyu, Theoretical study of single-bonded nitrogen cluster-type molecules, *Int. J. Quantum Chem.*, 1999, **73**, 349–356.

28 M. Tobita and R. J. Bartlett, Structure and stability of N_6 isomers and their spectroscopic characteristics, *J. Phys. Chem. A*, 2001, **105**, 4107–4113.

29 Y. Ren, X. Wang, N.-B. Wong, A.-M. Tian, F.-j. Ding and L. Zhang, Theoretical study of the N_{10} clusters without double bonds, *Int. J. Quantum Chem.*, 2001, **82**, 34–43.

30 L. P. Cheng, S. Li and Q. S. Li, Polynitrogen clusters containing five-membered rings, *Int. J. Quantum Chem.*, 2004, **97**, 933–943.

31 H. Zhou, W. Zheng, X. Wang, Y. Ren, N.-B. Wong, Y. Shu and A. Tian, A Gaussian-3 investigation on the stabilities and bonding of the nine N_{10} clusters, *J. Mol. Struct.*, 2005, **732**, 139–148.

32 B. Tan, X. Long and J. Li, The cage strain energies of high-energy compounds, *Comput. Theor. Chem.*, 2012, **993**, 66–72.

33 B. Tan, M. Huang, X. Long, J. Li, X. Yuan and R. Xu, From planes to cluster: the design of polynitrogen molecules, *Int. J. Quantum Chem.*, 2015, **115**, 84–89.

34 L. Türker, Contemplation on some cyclic N_8 isomers-A DFT treatment, *Def. Technol.*, 2018, **14**, 19–27.

35 L. Türker, A density functional study on some cyclic N_{10} isomers, *Def. Technol.*, 2019, **15**, 154–161.

36 O. V. Mikhailov and D. V. Chachkov, Molecular structures and thermodynamics of stable N_4, N_6 and N_8 neutral poly-nitrogens according to data of QCISD(T)/TZVP method, *Chem. Phys. Lett.*, 2020, 137594.

37 Q. S. Li, L. J. Wang and W. G. Xu, Structures and stability of N_9, N_9^- and N_9^+ clusters, *Theor. Chem. Acc.*, 2000, **104**, 67–77.

38 Y. D. Liu, J. F. Zhao and Q. S. Li, Structures and stability of N_7^+ and N_7^- clusters, *Theor. Chem. Acc.*, 2002, **107**, 140–146.

39 C.-K. Law, W.-K. Li, X. Wang, A. Tian and N. Wong, A Gaussian-3 study of N_7^+ and N_7^- isomers, *J. Mol. Struct.*, 2002, **617**, 121–131.

40 Y. H. Liang, Q. Luo, M. Guo and Q. S. Li, What are the roles of N_3 and N_5 rings in designing polynitrogen molecules?, *Dalton Trans.*, 2012, **41**, 12075–12081.

41 M. J. Greschner, M. Zhang, A. Majumdar, H. Liu, F. Peng, J. S. Tse and Y. Yao, A new allotrope of nitrogen as high-energy density material, *J. Phys. Chem. A*, 2016, **120**, 2920–2925.

42 S. Liu, L. Zhao, M. Yao, M. Miao and B. Liu, Novel All-Nitrogen Molecular Crystals of Aromatic N_{10}, *Adv. Sci.*, 2020, **7**, 1902320.

43 S. V. Bondarchuk, Bipentazole (N_{10}): A Low-Energy Molecular Nitrogen Allotrope with High Intrinsic Stability, *J. Phys. Chem. Lett.*, 2020, **11**(14), 5544–5548.

44 R. Engelke and J. R. Stine, Is N_8 cubane stable?, *J. Phys. Chem.*, 1990, **94**, 5689–5694.

45 K. M. Dunn and K. Morokuma, Transition state for the dissociation of tetrahedral N_4, *J. Chem. Phys.*, 1995, **102**, 4904–4908.

46 M. T. Nguyen and T.-K. Ha, Azidopentazole is Probably the Lowest-Energy N_8 Species-A Theoretical Study, *Chem. Ber.*, 1996, **129**, 1157–1159.

47 S. Evangelisti and L. Gagliardi, A complete active-space self-consistent-field study on cubic N_8, *Il Nuovo Cimento D*, 1996, **18**, 1395–1405.

48 L. Gagliardi, S. Evangelisti, V. Barone and B. O. Roos, On the Dissociation of N_6 into $3N_2$ Molecules, *Chem. Phys. Lett.*, 2000, **320**, 518–522.

49 L. Gagliardi, S. Evangelisti, A. Bernhardsson, R. Lindh and B. O. Roos, Dissociation reaction of N_8 azapentalene to $4N_2$: a theoretical study, *Int. J. Quantum Chem.*, 2000, 77, 311–315.

50 G. Chung, M. W. Schmidt and M. S. Gordon, An *ab initio* study of potential energy surfaces for N_8 isomers, *J. Phys. Chem. A*, 2000, **104**, 5647–5650.

51 L. J. Wang, W. G. Xu and Q. S. Li, Stability of N_8 isomers and isomerization reaction of $N_8(C_{2v})$ to $N_8(C_s)$, *J. Mol. Struct.*, 2000, **531**, 135–141.

52 M. T. Nguyen and T.-K. Ha, Decomposition mechanism of the polynitrogen N_5 and N_6 clusters and their ions, *Chem. Phys. Lett.*, 2001, **335**, 311–320.

53 T. Klapötke and R. Harcourt, The interconversion of N_{12} to N_8 and two equivalents of N_2, *J. Mol. Struct.*, 2001, **541**, 237–242.

54 Q. S. Li and L. J. Wang, A Quantum Chemical Theoretical Study of Decomposition Pathways of $N_9(C_{2v})$ and $N_9^+(C_{2v})$ Clusters, *J. Phys. Chem. A*, 2001, **105**, 1203–1207.

55 D. L. Strout, Acyclic N_{10} fails as a high energy density material, *J. Phys. Chem. A*, 2002, **106**, 816–818.

56 M. D. Thompson, T. M. Bledson and D. L. Strout, Dissociation barriers for odd-numbered acyclic nitrogen molecules N_9 and N_{11}, *J. Phys. Chem. A*, 2002, **106**, 6880–6882.

57 L. J. Wang, P. G. Mezey and M. Z. Zgierski, Stability and the structures of Nitrogen clusters N_{10}, *Chem. Phys. Lett.*, 2004, **391**, 338–343.

58 V. Elesin, N. Degtyarenko, K. Pazhitnykh and N. Matveev, Modeling of synthesis and dissociation of the N_4 nitrogen cluster of D_{2h} symmetry, *Russ. Phys. J.*, 2009, **52**, 1224–1234.

59 M. Noyman, S. Zilberg and Y. Haas, Stability of polynitrogen compounds: the importance of separating the σ and π electron systems, *J. Phys. Chem. A*, 2009, **113**, 7376–7382.

60 B. Hirshberg and R. B. Gerber, Decomposition mechanisms and dynamics of N_6: Bond orders and partial charges along classical trajectories, *Chem. Phys. Lett.*, 2012, **531**, 46–51.

61 M. T. Nguyen, M. McGinn, A. Hegarty and J. Elguero, Can the pentazole anion (N_5^-) be isolated and/or trapped in metal complexes?, *Polyhedron*, 1985, **4**, 1721–1726.

62 S. Fau and R. J. Bartlett, Possible products of the end-on addition of N_3^- to N_5^+ and their stability, *J. Phys. Chem. A*, 2001, **105**, 4096–4106.

63 L. Gagliardi, G. Orlandi, S. Evangelisti and B. O. Roos, A theoretical study of the nitrogen clusters formed from the ions N_3^-, N_5^+, and N_5^-, *J. Chem. Phys.*, 2001, **114**, 10733–10737.

64 S. Fau, K. J. Wilson and R. J. Bartlett, On the Stability of $N_5^+N_5^-$, *J. Phys. Chem. A*, 2002, **106**, 4639–4644.

65 Q. S. Li and J. F. Zhao, A theoretical study on decomposition pathways of N_7^+ and N_7^- clusters, *J. Phys. Chem. A*, 2002, **106**, 5928–5931.

66 L. Gagliardi, S. Evangelisti, P.-O. Widmark and B. O. Roos, A theoretical study of the N_8 cubane to N_8 pentalene isomerization reaction, *Theor. Chem. Acc.*, 1997, **97**, 136–142.

67 Q. S. Li and Y. D. Liu, Theoretical studies of the N_6 potential energy surface, *J. Phys. Chem. A*, 2002, **106**, 9538–9542.

68 M. W. Schmidt, M. S. Gordon and J. A. Boatz, Cubic fuels?, *Int. J. Quantum Chem.*, 2000, **76**, 434–446.

69 L. Türker, Contemplation on Some Prismatic Polynitrogen Structures-A DFT Treatment, *Z. Anorg. Allg. Chem.*, 2019, **645**, 1118–1126.

70 M. W. Schmidt, K. K. Baldridge, J. A. Boatz, S. T. Elbert, M. S. Gordon, J. H. Jensen, S. Koseki, N. Matsunaga, K. A. Nguyen, S. Su, *et al.*, General atomic and molecular electronic structure system, *J. Comput. Chem.*, 1993, **14**, 1347–1363.

71 H. Werner, P. Knowles, G. Knizia, F. Manby, M. Schütz, P. Celani, W. Györffy, D. Kats, T. Korona, R. Lindh, *et al.*, *MOLPRO, version 2015.1, a package of ab initio programs*. University of Cardiff Chemistry Consultants (UC3), Cardiff, Wales, UK2015.

72 W. Kohn and L. J. Sham, Self-consistent equations including exchange and correlation effects, *Phys. Rev.*, 1965, **140**, A1133.

73 F. Weigend and R. Ahlrichs, Balanced basis sets of split valence, triple zeta valence and quadruple zeta valence quality for H to Rn: Design and assessment of accuracy, *Phys. Chem. Chem. Phys.*, 2005, **7**, 3297–3305.

74 Y. Zhao and D. G. Truhlar, The M06 suite of density functionals for main group thermochemistry, thermochemical kinetics, noncovalent interactions, excited states, and transition elements: two new functionals and systematic testing of four M06-class functionals and 12 other functionals, *Theor. Chem. Acc.*, 2008, **120**, 215–241.

75 R. Peverati and D. G. Truhlar, *Communication: A global hybrid generalized gradient approximation to the exchange-correlation functional that satisfies the second-order density-gradient constraint and has broad applicability in chemistry*. 2011.

76 R. Peverati and D. G. Truhlar, M11-L: a local density functional that provides improved accuracy for electronic structure calculations in chemistry and physics, *J. Phys. Chem. Lett.*, 2012, **3**, 117–124.

77 Y. Zhao and D. G. Truhlar, Exploring the limit of accuracy of the global hybrid meta density functional for main-group thermochemistry, kinetics, and noncovalent interactions, *J. Chem. Theory Comput.*, 2008, **4**, 1849–1868.

78 N. Mardirossian and M. Head-Gordon, How accurate are the Minnesota density functionals for noncovalent interactions, isomerization energies, thermochemistry, and barrier heights involving molecules composed of main-group elements?, *J. Chem. Theory Comput.*, 2016, **12**, 4303–4325.

79 B. M. Bode and M. S. Gordon, MacMolPlt: a graphical user interface for GAMESS, *J. Mol. Graphics Modell.*, 1998, **16**, 133–138.

80 M. Silva, F. Silva, B. Galvão, J. Braga and J. Belchior, A genetic algorithm survey on closed-shell atomic nitrogen clusters employing a quantum chemical approach, *J. Mol. Model.*, 2018, **24**, 196.

81 C. Gonzalez and H. B. Schlegel, Reaction path following in mass-weighted internal coordinates, *J. Phys. Chem.*, 1990, **94**, 5523–5527.

82 R. J. Bartlett, Coupled-cluster approach to molecular structure and spectra: a step toward predictive quantum chemistry, *J. Phys. Chem.*, 1989, **93**, 1697–1708.

83 R. J. Bartlett, J. Watts, S. Kucharski and J. Noga, Non-iterative fifth-order triple and quadruple excitation energy corrections in correlated methods, *Chem. Phys. Lett.*, 1990, **165**, 513–522.

84 K. Raghavachari, G. W. Trucks, J. A. Pople and M. Head-Gordon, A fifth-order perturbation comparison of electron correlation theories, *Chem. Phys. Lett.*, 1989, **157**, 479–483.

85 T. H. Dunning Jr, Gaussian basis sets for use in correlated molecular calculations. I. The atoms boron through neon and hydrogen, *J. Chem. Phys.*, 1989, **90**, 1007–1023.

86 R. A. Kendall, T. H. Dunning Jr and R. J. Harrison, Electron affinities of the first-row atoms revisited. Systematic basis sets and wave functions, *J. Chem. Phys.*, 1992, **96**, 6796–6806.

87 T. B. Adler, G. Knizia and H.-J. Werner, A simple and efficient CCSD(T)-F12 approximation, *J. Chem. Phys.*, 2007, **127**, 221106.

88 G. Knizia, T. B. Adler and H.-J. Werner, Simplified CCSD(T)-F12 methods: Theory and benchmarks, *J. Chem. Phys.*, 2009, **130**, 054104.

89 K. P. Katin, V. B. Merinov, A. I. Kochaev, S. Kaya and M. M. Maslov, All-nitrogen cages and molecular crystals: Topological rules, stability, and pyrolysis paths, *Computation*, 2020, **8**, 91.

90 I. Y. Zhang, J. Wu and X. Xu, Extending the reliability and applicability of B3LYP, *Chem. Commun.*, 2010, **46**, 3057–3070.

91 Y. Zhao, N. González-García and D. G. Truhlar, Benchmark database of barrier heights for heavy atom transfer, nucleophilic substitution, association, and unimolecular reactions and its use to test theoretical methods, *J. Phys. Chem. A*, 2005, **109**, 2012–2018.

92 M. Evans and M. Polanyi, On the introduction of thermodynamic variables into reaction kinetics, *Trans. Faraday Soc.*, 1937, **33**, 448–452.